Atomic-scale simulations of strain localization in three-dimensional model amorphous solids

Yunfeng Shi and Michael L. Falk
Department of Materials Science and Engineering, University of Michigan, Ann Arbor, Michigan 48109-2136, USA
(Received 27 March 2006; published 2 June 2006)

Molecular-dynamics simulations of the mechanical properties of three different three-dimensional metallic glass analogs reveal that each exhibits a transition from homogeneous flow to localized flow as the quench rate used to produce the glass is decreased. The solid samples are tested in uniaxial compression over more than an order of magnitude range of strain rates. Three different systems are studied including one single-component glass former and two binary alloys. The strain rate sensitivity of the localization changes sign at a critical cooling rate, implying a discontinuous transition in mechanical properties in the low loading rate limit. Analysis of the short-range order using a generalization of the Frank-Kasper criterion reveals that the short-range order is depleted in the shear band in two of the three systems. Moreover, the homogeneous to inhomogeneous deformation transition in the mechanical properties is found to coincide with the percolation of an identifiable aspect of the short-range order in those two systems. The third system studied, the Kob-Anderson glass, is hypothesized not to be amenable to the methods typically used to characterize short-range order due to its non-hard-sphere nature.

DOI: 10.1103/PhysRevB.73.214201 PACS number(s): 62.20.Fe, 61.43.−j

I. INTRODUCTION

When a solid is plastically deformed, it can exhibit either homogenous deformation, during which the plastic strain is uniform throughout the specimen, or localized deformation, during which plastic strain is confined in thin regions called shear bands. Strain localization occurs spontaneously in a variety of material systems including fine-grained alloys, metallic glasses, polymers, granular media, foams, and colloids.[1–5] Physically based theories for localization are critical for predicting fracture in amorphous solids, rheological response, structural stability of granular media, and energy dissipation in geophysical processes.

It is commonly believed that strain localization arises from loss of stability. Cases like adiabatic shear banding that arise due to a thermoplastic instability are thought to be well understood.[6,7] However, there is no equivalent theory for many other systems. One such system is metallic glass. Metallic glass is a relatively new material that exhibits great promise for many applications due to its high elastic limit, high specific strength, and high restitution coefficient.[8,9] However, spontaneous localization of strain presents the dominant failure mode for metallic glass. Particularly under uniaxial tension the tendency for metallic glass to undergo localized deformation often results in dramatic failure via fracture along a single shear band.[10] This failure mode can prevent any apparent hardening in tension, limiting the utility of metallic glasses for structural applications. Current theoretical concepts regarding softening and localization in these materials have relied on the concepts of free volume[11] and shear transformation zones.[12,13] In free volume theories[11,12,14] excess free volume generated during deformation lowers the viscosity of the glass resulting in softening and localization.[14] Closely related shear transformation zone theories focus on the micromechanisms of shear.[12] Both theories use a similar language of deformation kinetics pioneered by Eyring[15] to describe the evolution of the glass microstructure. These models have been used to understand shear softening and shear thinning,[16] and to analyze data on the emergence of localization.[17] However, none of the current theories can be used to directly model the nucleation and propagation of shear bands, and many of the parameters in the current theories cannot unambiguously be related to specific atomic scale structures or the thermomechanical history of the glass.

Experimental techniques such as positron-annihilation spectroscopy can reveal the open volume of metallic glass but with rather poor spatial resolution.[18,19] Several advanced transmission electron microscopy (TEM) and x-ray-diffraction techniques have been developed to study amorphous solids: (i) fluctuation electron microscopy (FEM), which aims to probe the medium range ordering (MRO) by analyzing the variation of the contrast of dark-field images with different degree of coherency of the electron beam;[20–25] (ii) quantitative high-resolution transmission electron microscopy (HRTEM), which has been used to map the nanometer size voids inside the shear bands;[26–28] (iii) extended x-ray-absorption fine structure (EXAFS) which can provide species-specific local environment information.[29] The third technique is of particular interest because it can be used to reconstruct the three-dimensional atomic configurations by using reverse Monte Carlo (RMC) methods.[30,31] However, an experimental structural characterization technique that can provide unambiguous structural information at the atomic scale is still lacking.

Atomic scale simulations, particularly molecular dynamics (MD) that can reveal dynamics of the physical process, play an increasingly crucial role in answering fundamental questions in materials science. This is made possible partially by the unprecedented computing power and readily available algorithms that are capable of modeling many material systems under a variety of conditions. In the simulation work that has been undertaken regarding the mechanical behavior of metallic glasses, qualitative agreement between simulation observations and experimental results is observed in the general behavior of stress-strain curves, yielding and cyclic loading behaviors.[32–40] It should be noted that, be-

cause a typical experimentally observed shear band width in a metallic glass is on the order of 10–20 nm, the spatial dimension of simulation box has to be considerably larger to contain a shear band than to examine homogeneous elastic or plastic response. Perhaps for this reason there has been relatively little simulation work on strain localization of disordered systems[35,39,41–43] as compared to experimental or theoretical investigations. In particular, recent work by Bailey, Schiotz, and Jacbosen[39] have observed that in their simulations shear bands do not arise as the result of a thermal softening instability and that the shear banded region is not characterized by a decrease in local density. The latter results call into question the utility of free volume, closely related to the local density, as a useful way to characterize the structural changes that accompany strain localization in metallic glasses on the atomic scale. Only a few of the atomistic studies to date have investigated the effect of quenching rate on mechanical response.[42,43] The thermal history of the glass affects the structure of the glass, and therefore would reasonably be expected to affect mechanical behavior. We also consider the effect of strain rate and, in the process, perform multiple simulations to account for issues of sample-to-sample variation inherent in the study of disordered systems.

To investigate the strain localization behavior of amorphous solids, we previously performed molecular-dynamics simulations of uniaxial tensile loading[43] and nanoindentation[44] on two-dimensional binary Lennard-Jones systems. A transition in the mechanical behavior was observed to occur in the quasistatic limit. Homogenous deformation was predicted for quickly quenched glasses while localized deformation was predicted for slowly quenched glasses. This transition was found to coincide with the k-core percolation of quasicrystal-like short range order (SRO). Furthermore, the fact that the material inside the shear band has a lower degree of SRO than the undeformed material indicates the instability arises from structural disordering. While the results of these two-dimensional simulations are compelling, in a more realistic three-dimensional system the additional degrees of freedom of the atoms could significantly affect the dynamics of the physical process. Some atomic rearrangements could be easier in three dimensions due to the otherwise prohibited motion in the perpendicular direction. For two-dimensional systems, the preferred packing locally and globally is the same: equilateral triangles. This is why atomic size mismatch has to be included to form a glass.[45] However, for three-dimensional systems, the locally preferred packing, tetrahedra, cannot on its own constitute the global ground-state structure. Therefore it is of interest to test whether the observations made in two-dimensional systems hold in three dimensions. In this work, three different three-dimensional systems are investigated through mechanical tests and analysis procedures similar to those carried out in Ref. 43.

II. MOLECULAR-DYNAMICS SIMULATIONS

A. Potential models

Three different model glass formers are investigated in this work to examine the extent to which our prior observations in two-dimensional systems are generic.[43,44] The first model utilizes the Dzugutov potential (DZ) to create a one-component glass in three dimensions. The DZ potential is described by the function

$$U(r) = A(r^{-m} + B)\exp\left(\frac{c}{r-a}\right)\Theta(a-r) + B\exp\left(\frac{d}{r-b}\right)\Theta(b-r). \quad (1)$$

The parameters m, A, B, a, b, c, and d are chosen as described in Ref. 46 and Θ represents the Heaviside step function which enforces the short-range nature of each of the terms. All quantities are measured in reduced units: σ, a length scale approximately proportional to 88.5% of the bond length, and ε, an energy scale approximately proportional to 1.72 times the binary interaction energy.[46] These are chosen to facilitate comparison to the widely used Lennard-Jones system which is described below. By assuming particle mass is m_0, the reduced time unit is $t_0=\sigma\sqrt{m_0/\varepsilon}$. This potential features a maximum at the distance at which neighboring atoms would reside in order to form fcc, bcc, or hcp crystals. When cooled from the melt under zero pressure, the system does not form these crystal phases; however, dodecagonal quasicrystals or Frank-Kasper crystals can be formed if cooling is slow enough.[47] Under higher cooling rates, glasses are formed. The mode coupling temperature of this system $T_{MCT}=0.4\varepsilon/k$.[48] This sets an upper bound for the glass transition temperature.

The second simulated glass is a Wahnstrom (WA) binary Lennard-Jones system.[49] We will refer the two species as A and B. Atoms interact via a standard 12-6 Lennard-Jones potential:

$$U_{\alpha\beta}(r) = 4\varepsilon_{\alpha\beta}\left[\left(\frac{\sigma_{\alpha\beta}}{r}\right)^{12} - \left(\frac{\sigma_{\alpha\beta}}{r}\right)^{6}\right], \quad (2)$$

where α and β represent the species of the interacting atoms; $\varepsilon_{\alpha\beta}$ represents the energy of the bond and $\sigma_{\alpha\beta}$ provides a length scale, the distance at which the interaction energy is zero. We choose ε_{AA}, σ_{AA}, and m_B as the reduced units for energy, length, and mass. The time unit is $t_0=\sigma_{AA}\sqrt{m_0/\varepsilon_{AA}}$. The parameters are $\varepsilon_{AA}=1.0$, $\varepsilon_{BB}=1.0$, $\varepsilon_{AB}=\varepsilon_{BA}=1.0$, $\sigma_{AA}=1.0$, $\sigma_{BB}=5/6$, $\sigma_{AB}=\sigma_{BA}=11/12$, $m_A=2$, and $m_B=1$. Interactions are neglected beyond a cutoff set by the distance at which the interaction potential falls below a critical value, $U_{\alpha\beta}(r_{c,\alpha\beta})=0.0163\varepsilon_{AA}$, such that $r_{c,AA}$ is 2.5 σ_{AA}, and energy calculations are adjusted accordingly. This system has been used by others to study dynamical heterogeneity in the supercooled liquid regime[50] and by one of the authors to investigate plastic deformation in the glassy state.[51,52]

The third glass forming system studied here is a Kob-Andersen (KA) binary Lennard-Jones system. The two species, which will again be referred to as A and B, also interact via Eq. (2). We choose ε_{AA}, σ_{AA}, and m_A as the reduced units for energy, length, and mass for this system. The time unit is $t_0=\sigma_{AA}\sqrt{m_0/\varepsilon_{AA}}$. The parameters for KA are $\varepsilon_{AA}=1.0$, $\varepsilon_{BB}=0.5$, $\varepsilon_{AB}=\varepsilon_{BA}=1.5$, $\sigma_{AA}=1.0$, $\sigma_{BB}=0.88$, $\sigma_{AB}=\sigma_{BA}=0.8$, $m_A=1$, and $m_B=1$. Interactions are neglected beyond a cutoff

TABLE I. Cooling schedules for DZ, WA, and KA systems.

System	N (atoms)	$L_x \times L_y \times L_z$ (σ^3)	T_{MCT} (ε/k)	t_{cool} (t_0)	T_i (ε/k)	T_f (ε/k)	P_i (ε/σ^3)	P_f (ε/σ^3)	ρ_i ($1/\sigma^3$)	Number of samples
DZ-1	112,000	$74\times114\times16$	0.4	1000	1.0	0.030	6.0	0.0	0.84	4
DZ-2	112,000	$74\times114\times16$	0.4	2000	1.0	0.030	6.0	0.0	0.84	5
DZ-3	112,000	$74\times114\times16$	0.4	5000	1.0	0.030	6.0	0.0	0.84	5
DZ-4	112,000	$74\times114\times16$	0.4	7500	1.0	0.030	6.0	0.0	0.84	4
DZ-5	112,000	$74\times114\times16$	0.4	10000	1.0	0.030	6.0	0.0	0.84	8
WA-1	144,000	$70\times105\times15$	0.57	100	1.2	0.036	13.3	0.0	1.28	3
WA-2	144,000	$70\times105\times15$	0.57	1000	1.2	0.036	13.3	0.0	1.28	3
WA-3	144,000	$70\times105\times15$	0.57	5000	1.2	0.036	13.3	0.0	1.28	9
WA-4	144,000	$70\times105\times15$	0.57	10000	1.2	0.036	13.3	0.0	1.28	9
WA-5	144,000	$70\times105\times15$	0.57	40000[a]	1.2	0.036	13.3	0.0	1.28	5
KA-1	144,000	$72\times108\times15$	0.435	100	0.87	0.030	8.5	0.0	1.20	3
KA-2	144,000	$72\times108\times15$	0.435	1000	0.87	0.030	8.5	0.0	1.20	3
KA-3	144,000	$72\times108\times15$	0.435	10000	0.87	0.030	8.5	0.0	1.20	6
KA-4	144,000	$72\times108\times15$	0.435	20000	0.87	0.030	8.5	0.0	1.20	6

[a]This is an estimated cooling time for a three-step cooling schedule that is comparable to other one-step cooling schedules (details in Table II).

set by the distance at which the interaction potential falls below a critical value, $U_{\alpha\beta}(r_{c,\alpha\beta})=0.0163\varepsilon_{AA}$, such that $r_{c,AA}$ is $2.5\sigma_{AA}$.

In order to simplify discussions that follow, we use reduced units ε, σ, m, and t_0 for energy, length, mass and time to express our results for all three systems. The exact values of those physical quantities are system dependent as described above.

B. Preparation of glasses

We choose to simulate N atoms in a box of size $L_x \times L_y \times L_z$ where L_z is much smaller than the other two dimensions. Information about the simulation systems for all three potentials is summarized in Table I. This slab geometry is used to maximize the spatial dimension in the X-Y plane, as in Ref. 39. We prepare the glassy samples in the following way. We start from well equilibrated liquid at initial temperature T_i and pressure P_i. Then the system is quenched down to a very low final temperature T_f and pressure P_f over a chosen time period (cooling time t_{cool}) by constantly reducing the temperature and pressure. The temperature is controlled by using a Nose-Hoover thermostat with a varying heat bath temperature.[53] The pressure is controlled by a Parrinello-Rahman barostat with a varying externally applied pressure.[54,55] The starting number density of the liquid is ρ_i. This and the mode coupling temperatures (T_{MCT}) for all three potentials for each particular initial number density are also listed in Table I. T_i is at least double T_{MCT} so that a relatively short amount of time is needed to achieve thermal equilibrium. The temperature of the glassy solid (T_f) is around 3% of that of the T_{MCT} so that thermal effects are minimized during the compression tests. For the WA and KA systems, a glass is formed under all quenching rates investigated here. However, for the DZ system, quasicrystals and sometimes even bcc crystallites can be precipitated for low quenching rates. Discontinuities in the potential energy versus temperature are evident for slowly cooled DZ samples. These correspond to the formation of dodecagonal quasicrystals as confirmed by the structural analysis:[47] for samples with cooling time longer than 10 000 t_0, a 12-fold symmetry axis indicates the existence of dodecagonal quasicrystals. Therefore this is the maximum cooling time we can use and still obtain a glass for the DZ system. The cooling times for the DZ samples are 1000, 2000, 5000, 7500, 10 000 t_0 for DZ-1 through DZ-5 as in Table I. The cooling times for the WA samples are 100, 1000, 5000, 10 000, 40 000 (effective) t_0 for WA-1 through WA-5 as in Table I. For the slowest cooling for the WA system, we use a three stage quenching schedule (Table II) to maximize the cooling time while the temperature is near the glass transition temperature. A one-stage quench spends about one quarter of the time around the glass transition (step II in Table II). Therefore we consider the effective cooling time for WA-5 to be about 40 000 t_0. This practice is used to reduce the computing time. The cooling times for the KA system are 100, 1000, 10 000, 20 000 t_0 for KA-1 through KA-4 as in Table I. Three to nine independent samples for each quenching schedule are employed to examine sample to sample variations. The average potential energy per atom

TABLE II. Three-step cooling schedule for WA-5.

	T_{start} (ε/k)	T_{end} (ε/k)	P_{start} (ε/σ^3)	P_{end} (ε/σ^3)	Cooling Time for WA-5 (t_0)
Step I	1.2	0.73	13.3	7.98	100
Step II	0.73	0.45	7.98	4.73	10000
Step III	0.45	0.036	4.73	0.00	100

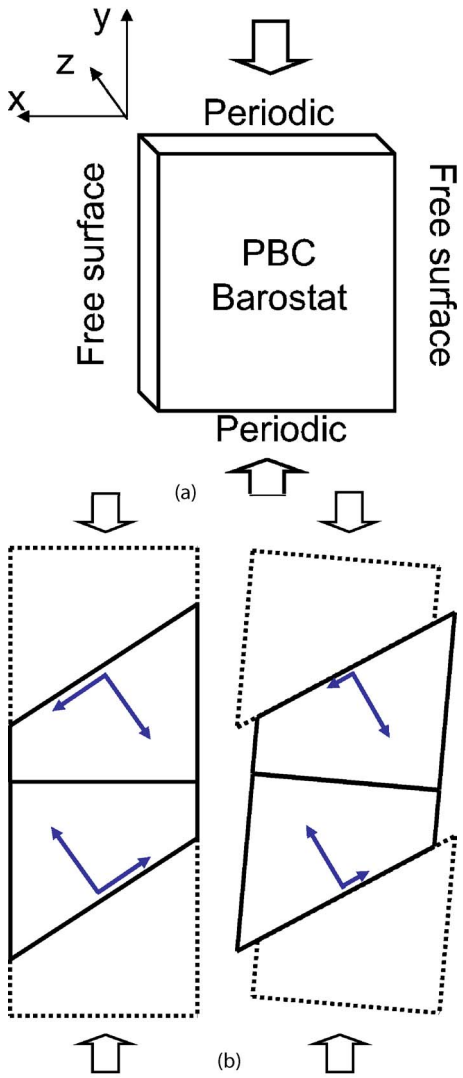

FIG. 1. (Color online) Illustration of the test geometry (a) and the slip with rotation (b) for uniaxial compression. Materials between the slip plane, denoted by the tilted line in (b), and its image are considered to be the simulation system. The arrows represent the normal and tangential forces on the slip plane.

before mechanical tests is used to quantify the structural stability of the glass. Samples quenched at higher rates exhibit higher potential energy.

The geometry for the uniaxial compression test is illustrated in Fig. 1(a). During mechanical tests the Y axis is the uniaxial compression direction. The strain is applied homogenously throughout the sample with periodic boundary conditions imposed along both X-Y planes and Z-X planes, although the material response is not constrained to be homogeneous. Y-Z planes are free surfaces in order to allow shear band slip. There are two facts that suggest the presence of the free surfaces are important for relieving the structural constraint, but do not in themselves account for the localized deformation behavior: (i) the deformation does not necessarily initiate at the surfaces; (ii) simple shear tests using Lees-Edwards boundary conditions without surfaces show very similar localization behavior.[56] Thus we feel that these simulations show a more convincing demonstration of spontaneous localization from the bulk than simple shear simulations that utilize constrained bounding walls which could potentially induce localized deformation.[41] Next we consider the rotation of the system that accompanies shear band slip. For the sake of discussion, we consider the system between the shear band and the next shear band image as shown in Fig. 1(b). This system is equivalent to the original system due to the periodic boundary condition. Because the shear band normally forms at an angle approximately 45° to the loading direction, there is a net torque resulting from the normal stress. Before yielding, this torque is balanced by the torque of the friction force on the sliding surface. However, when slip occurs, the friction force drops, and the system is rotated by the normal stress torque. The rotation of the system is important because it allows shear band propagation while maintaining the lateral displacement of the top of the system relative to the bottom.

Since the sample is a thin slab, the net stress in the thickness direction, $\bar{\sigma}_{zz}$, is maintained zero by coupling to a barostat. No thermostat is used during compression. Six strain rates are used in this study: 0.0005, 0.0002, 0.0001, 0.00005, 0.000 02, and 0.000 01 t_0^{-1}.

C. Uniaxial tensile tests

Figure 2 shows representative compressive stress strain curves for the shortest and longest cooling times at the lowest strain rate for each of the three systems. For samples produced at the longer cooling times the stress reaches a higher maximum and then suddenly drops. This is followed by a more steady flow regime during which some serrations are evident. The sudden drops are caused by the formation of shear bands. However, for samples produced with short cooling time, the stress strain curves are rather smooth and the behavior is close to the ideal elastic–perfectly plastic response. Figure 3 shows typical systems compressed by 10% strain with atoms colored by the local value of the deviatoric shear strain. The deviatoric shear strain is obtained through a least-square fitting of the atomic displacements of neighboring atoms within a cutoff distance.[13] This cutoff distance is 3σ for all three systems. In Ref. 43, we introduced a quantity we called the deformation participation ratio (DPR) in order to quantify the degree of localization apparent in Fig. 3. The definition of DPR is the fraction of atoms that have a local deviatoric shear strain larger than the nominal shear strain for the whole system. For the case of ideally localized deformation in large systems, only a small fraction of the material carries the plastic deformation. Therefore the DPR has a lower bound of the shear band width divided by the system size for an ideally localized deformation. For the case of ideally homogenous deformation, atoms have equal probability to have a local strain larger than the nominal shear strain or smaller than the nominal shear strain. Therefore the DPR has an upper bound of 0.5 for ideally homogenous deformation. Following the same analysis as in Ref. 43, we obtained DPR at 10% strain for samples with different cooling rates and different strain rates as shown in Fig. 4. In all cases the

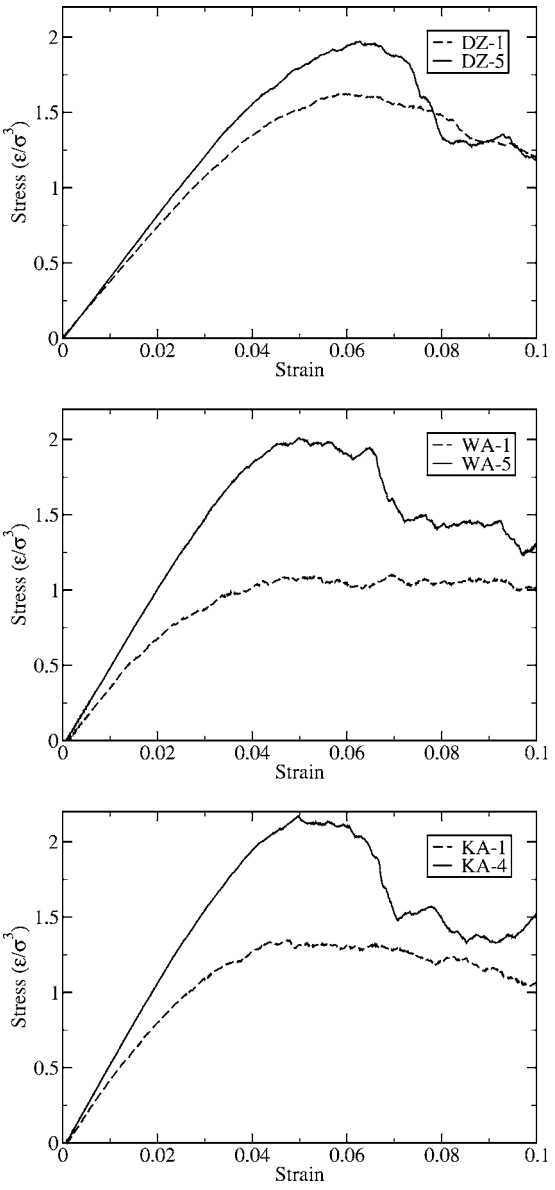

FIG. 2. Stress-strain curves for DZ (a), WA (b), and KA (c) systems at the lowest strain rate $0.000\,01 t_0^{-1}$. The broken lines represent samples produced with short cooling time (DZ-1, WA-1, and KA-1) and solid lines represent samples produced with long cooling time (DZ-5, WA-5, and KA-4).

DPR is lower in the samples that start at lower potential energy, indicating localization is enhanced in the more slowly quenched samples. Additionally, in all cases there is a crossover in the strain rate dependence of the DPR. For samples produced at high cooling rates, lower strain rate compression tests have higher DPR than higher strain rate tests. However, for samples with low cooling rates, lower strain rate compression tests have lower DPR. We quantify this utilizing a power-law relation to model DPR as a function of strain rate:

$$\mathrm{DPR} = A\dot{\varepsilon}^m \tag{3}$$

Here $\dot{\varepsilon}$ is the strain rate, A is a positive constant, and m is the strain rate sensitivity of the DPR. The purpose of the power-law fit is solely to quantify the trend of the strain rate dependence. Note that since we are only interested in the trend, no term is included in Eq. (3) that restricts DPR within the bounds of 0.0–0.5. Quantifying the trend with respect to strain rate is important because the lowest strain rate we can access using atomic simulations is approximately $10^7\ \mathrm{s}^{-1}$. Although we cannot directly simulate the localization behavior in the quasistatic limit, we can predict the low rate behavior from an extrapolation of the accessible high strain rate simulation data. Thus the physical significance of m is that the sign of m determines the predicted localization behavior in the low strain rate limit. If m is positive then, in the quasistatic large system size limit, DPR will approach zero, which corresponds to localized deformation. On the other hand, if m is negative, DPR will increase as strain rate decreases and eventually attain the upper bound of 0.5, which corresponds to homogenous deformation. As shown in Fig. 5, m changes from negative to positive in all three potential systems. This indicates that there is a discontinuous transition of homogenous flow to localized deformation in the quasistatic limit depending on sample preparations. A similar transition was observed in our study of the two-dimensional binary system described in Ref. 43.

III. SRO STRUCTURAL CHARACTERIZATION

Figure 6 shows the pair-correlation functions for the shortest and longest cooling time for all three systems before mechanical tests. It is clear that the two-body correlation functions, particularly the radial distributions obtained through averaging, do not capture the subtle structural differences between samples that are prepared with different quenching rates. Therefore higher-order correlations have to be considered. The quasicrystal-like SRO characterization used in our previous two-dimensional investigations[43,44] provides a way to quantify the many-body correlations by utilizing the fact that the two-dimensional system in Ref. 43 has an underlying quasicrystalline state. Similarly, the DZ system also has a dodecagonal quasicrystalline state that is of the Frank-Kasper type and is mostly tetrahedrally close packed.[57] However, there is no corresponding known quasicrystalline state for WA and KA systems. Here our goal is to find a generic means to characterize SRO in three-dimensional systems. A natural starting point is the tetrahedral order. This is because tetrahedral packing represents the closest approach of four rigid spheres. Even more sophisticated approaches, such as *ab initio* calculations on Li-atom cluster packing, predict that the optimal structures are those that maximize the number of tetrahedra because the valence electrons prefer to localize in tetrahedral interstices.[45,58] Therefore, under hard-sphere assumptions, it seems generally true that an atom prefers to form as many tetrahedra as possible with its nearest neighbors to maximize the local packing efficiency. This argument is also supported by the fact that, for all three systems, the samples with the lowest quenching rates are 0.5–0.8 % more dense than the samples with the highest quenching rates. We will assume that in an ideal packing the center atom forms nothing but tetrahedra with its neighbors. For example, the icosahedral center forms

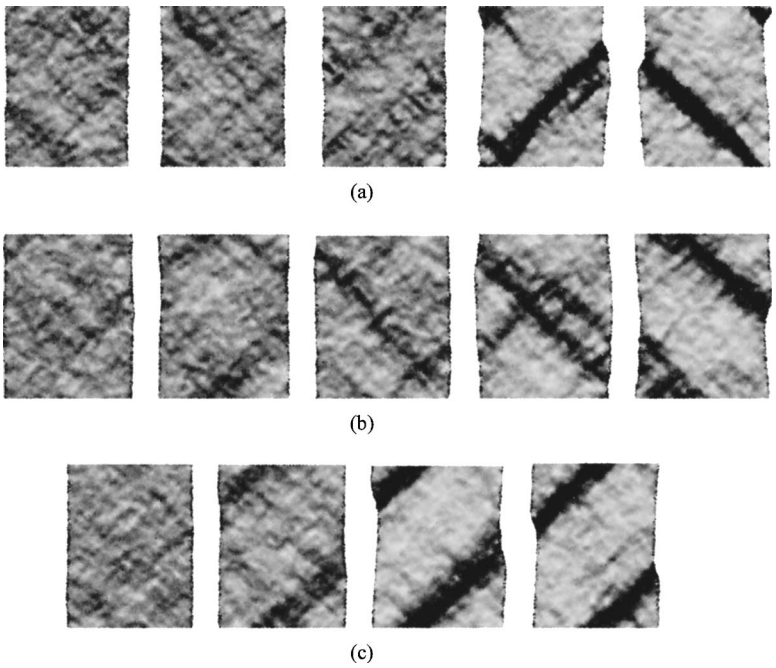

FIG. 3. Plastic deformation represented by deviatoric shear strain (projected to X-Y plane) of uniaxial compression samples at 10% strain at the lowest strain rate $0.000\,01t_0^{-1}$ for DZ-1 – DZ-5 from left to right as shown in (a); WA-1 – WA-5 from left to right as shown in (b); KA-1 – KA-4 from left to right as shown in (c). Atoms are colored according to the local deviatoric shear strain. Black represents strain larger than 20% while white represents 0% strain. The stress and strain curves of the systems with the shortest and longest cooling time for all three systems are plotted in Fig. 2.

20 tetrahedra with its neighboring vertices. This is equivalent to requiring that the faces of each coordination polyhedron, consisting of the near neighbors of each atom, are composed entirely of triangles. We will refer to the near neighbor atoms surrounding the central atom as the coordination shell.

By calculating the number of faces, edges, and vertices, a criterion for this ideal packing can be derived based on Euler's theorem:[59]

$$\sum_q (6-q)\nu_q = 12. \tag{4}$$

Here the surface coordination number q is defined for each atom in the coordination shell as the number of neighboring atoms also residing in the coordination shell. ν_q represents the number of atoms in the coordination shell with a surface coordination number q. We refer to atoms with a coordination shell satisfying Eq. (4) as atoms with triangulated coordination shell (TCS) SRO. Frank and Kasper[59] found four such triangulated coordination shells with coordination numbers of 12 (icosahedron), 14, 15, and 16 constraining the surface coordination number to be only 5 and 6 for nearly identical atoms. More configurations satisfy Eq. (4) if size-mismatch is allowed. Here we allow q to be any value for the sake of generality. In practice, q cannot be smaller than 3 except at the surface and cannot exceed 7 for all three systems investigated here. We use the average of the first and second peak position in the partial radial distribution function as the cutoffs for the first neighbor shell. The cutoff for the DZ system is about 1.48σ, which is close to 1.5σ used in other studies.[48] The cutoff for WA system is about 1.43, 1.32, 1.22σ for the AA, AB, and BB bonds, respectively. The cutoff for the KA system is about 1.45, 1.22, 1.32σ for the AA, AB, and BB bonds, respectively.

This topological criterion differs somewhat from the radius ratios calculated by Miracle, Sanders, and Senkov to maximize the packing efficiency of the first neighbor shell given a coordination number.[60] For comparison, the SRO criterion considered here requires the faces of the coordination polyhedron to be triangular without restricting the surface coordination number. On the other hand, the SRO criterion of Miracle *et al.* requires the surface coordination number to be the same without explicitly restricting the polyhedron faces. The essentially mean-field assumption that each atomic environment is identical leads to some configurations that seem to have no topological realization. For this reason we prefer the criterion presented here. Further studies are needed to illustrate which approach better represents packing in hard spheres and metallic glass alloys.

There are two other popular methods widely used to characterize the icosahedral order or crystalline order in liquids and glasses. In common neighbor analysis (CNA),[61] the structural unit identified is a pair of atoms, which is not an enclosed structure. Therefore it is not possible to associate a unique structural signature with an individual atom based on CNA. Instead, in the method above, we identify the complete first neighbor shell around each atom. Another important method to characterize the local environment is the bond orientational order analysis.[62] Different local atomic environments have different local bond order spectra. However, in order to obtain good statistics of the spectrum, one has to average over many atoms. Thus the spatial resolution is low. Furthermore, determining which type of local structure one atom belongs to based on its bond order spectrum is not trivial and often arbitrary cutoffs are used to make these distinctions.[63]

In Fig. 7, the number density of TCS SRO is plotted along with a deformation map in which atoms are colored by the local shear strain. For the DZ system and the WA system, the material inside the shear band has a significantly lower SRO than the undeformed material. Therefore the TCS SRO is effective for structurally characterizing the locations of shear bands in those two systems. This also indicates that the breakdown of this kind of SRO is critical to the instability

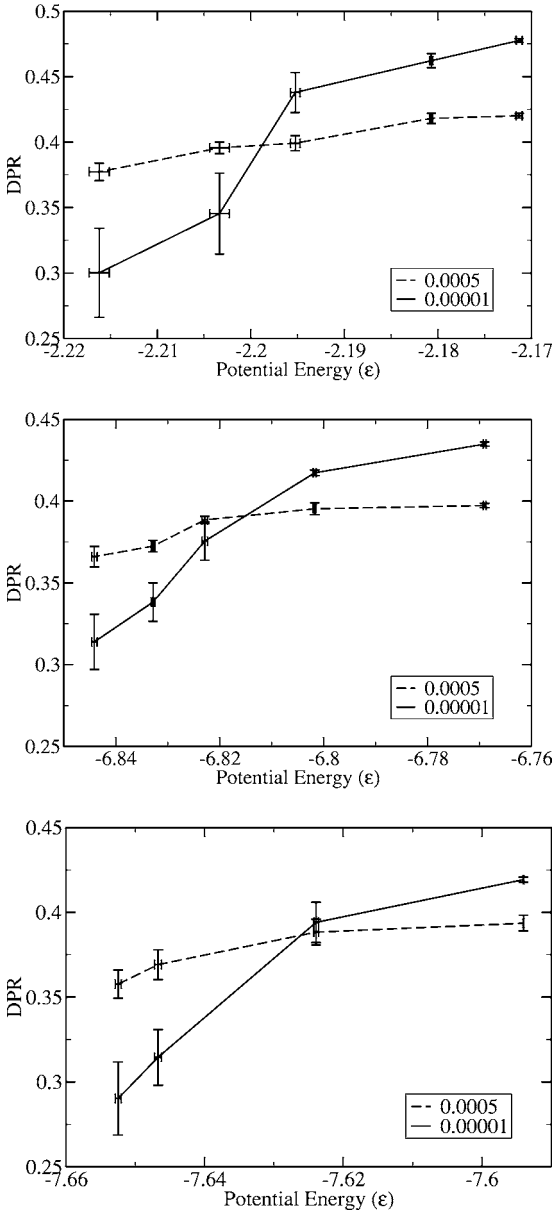

FIG. 4. Deformation participation ratio (DPR) measured at 10% strain plotted as a function of the potential energy per atom measured prior to the uniaxial compression tests for DZ (a), WA (b), and KA (c) systems. Data are shown for tests at the highest strain rate $0.0005t_0^{-1}$ (broken lines) and lowest strain rate $0.000\,01t_0^{-1}$ (solid lines).

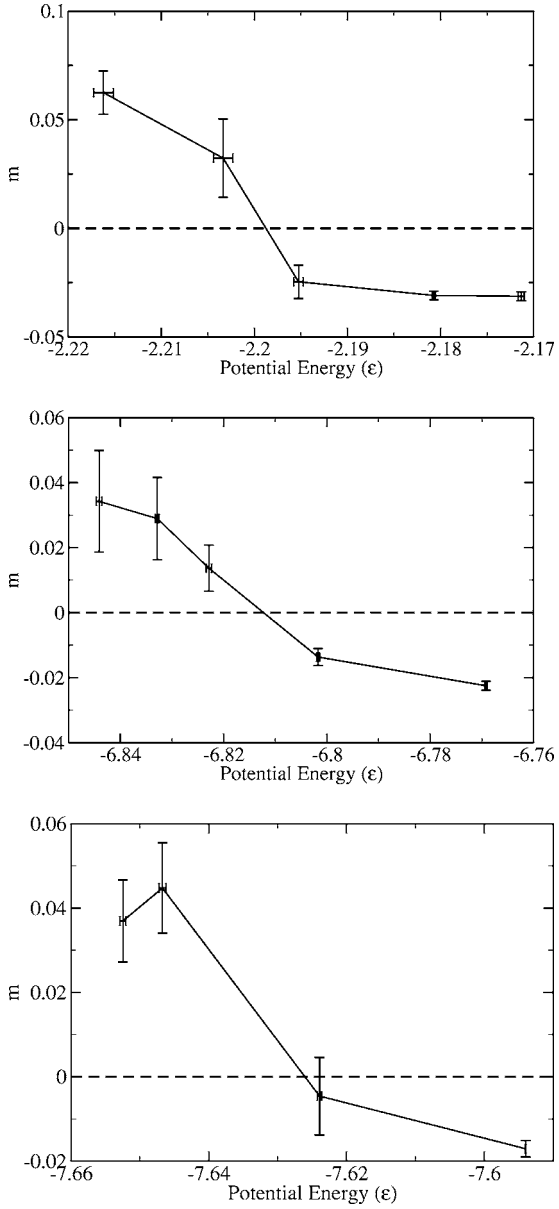

FIG. 5. Strain rate sensitivity m is plotted as a function of potential energy per atom of the sample measured prior to the mechanical test for DZ (a), WA (b), and KA (c) systems. A transition from negative to positive m occurs for all three systems.

that causes strain localization. This is analogous to our previous observation that quasicrystal-like SRO is depleted in shear bands during nanoindentation of a two-dimensional binary system.[44] However, for the KA system, there are no significant features in the density of TCS SRO similar to those in the deformation map. Therefore the success of this kind of SRO analysis depends on the specific nature of the potential and alloy system. For comparison, we included the number density maps in Fig. 7. These maps are equivalent to free volume calculations assuming a chemically homogeneous system since, in this case, the hard-sphere component v_0, subtracted to calculate the free volume, $v_f=\rho^{-1}-v_0$, is spatially uniform. Only the number density map in the DZ system shows recognizable features similar to the deformation map. It should be noted that there should be a correlation between the degree of TCS SRO as defined here and the number density, simply because this SRO definition is derived to correspond to efficient packing. However, the relatively small differences in number density are typically washed out by the local-density fluctuations. In order to obtain a better signal-to-noise ratio in analyzing the number density, one would need to average over a larger region of the material to get better statistics. This may not be possible on the narrow scale of a shear band width. Another significant draw back for number density is that it is very sensitive to the stress state since it couples to the dilatational strain.

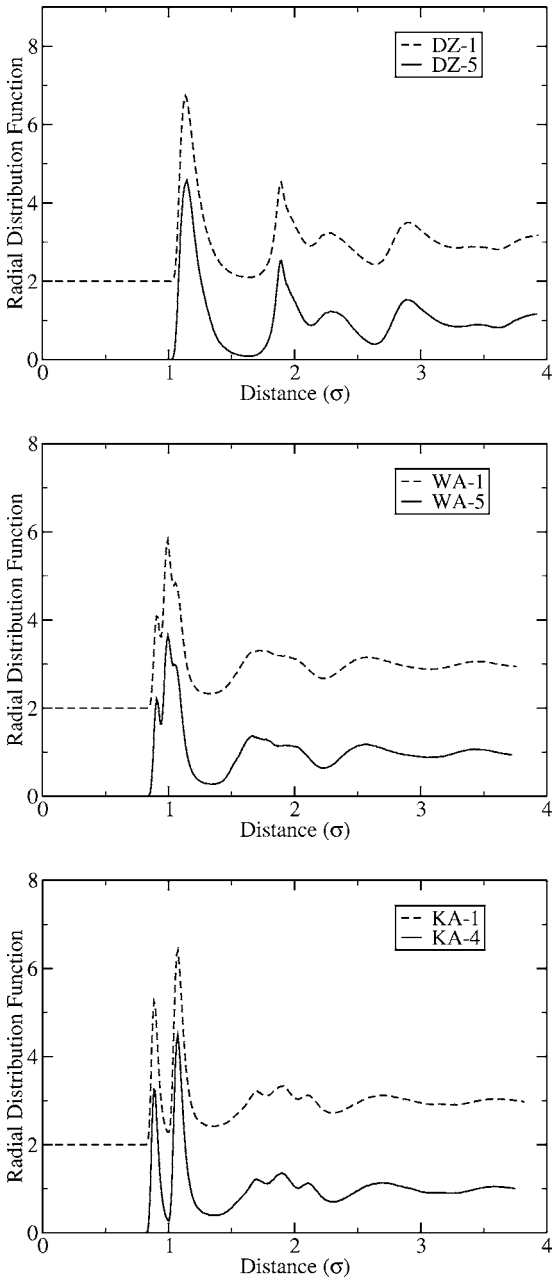

FIG. 6. Radial distribution function curves for (a) DZ-1 and DZ-5; (b) WA-1 and WA-5; (c) KA-1 and KA-4. The upper broken lines represent samples produced with the shortest cooling time and lower solid lines represent samples produced with the longest cooling time. The curves are shifted so that they will be distinguishable.

Therefore for our purposes SRO is a better structural characterization method than the number density or, by extension, free volume.

IV. PERCOLATION OF SRO

We have observed that in two dimensions k-core percolation of quasicrystal-like SRO (Ref. 43) coincides with the mechanical behavior transition. Here we want to investigate whether similar percolation of TCS SRO occurs in the three-

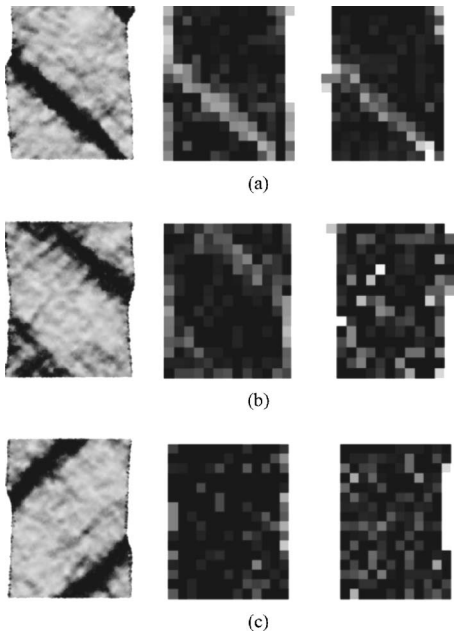

FIG. 7. Each row shows the distribution of plastic deformation (projected to X-Y plane) on the left, the density of TCS SRO (projected to X-Y plane) averaged over volume elements in the middle, and the average density over the same volume elements on the right. Row (a) is a DZ sample (DZ-5) and averaging is performed over volumes of size $6.3\times6.5\times16.3\sigma^3$; row (b) is a WA sample (WA-5) and averaging is performed over volumes of size $6.0\times6.4\times15.4\sigma^3$, and row (c) is a KA sample (KA-4) and averaging is performed over volumes of size $6.0\times6.3\times15.4\sigma^3$. All three samples have undergone a 10% strain compression at the lowest strain rate, $0.000\,01t_0^{-1}$. The color scheme of the distributions of plastic deformation is the same as in Fig. 3. For all TCS density maps, black represents SRO equal or larger than the average SRO; white represents zero SRO. For all number density maps, black represents the average local number density; white represents a density that is, 12% for (a), 3% for (b), and 5% for (c), lower than the average, respectively, to maximize contrast of the density maps.

dimensional systems. Following the connection criterion in Ref. 48, we define two atoms with TCS SRO to be connected if they share at least three atoms. This condition is equivalent to requiring the two TCS SRO coordination polyhedra to share a face or to interpenetrate.

For the DZ system, we observe that the TCS SRO percolates in all samples investigated, even those produced at the highest cooling rates. Thus we do not see a percolation transition of TCS SRO in DZ system corresponding to the transition in mechanical properties evident in Fig. 5. It should be noted that the Dzugutov potential deviates significantly from a hard-sphere model because of the energy maximum and the interactions extending beyond near neighbors. The fact that the Dzugutov potential strongly favors tetrahedral order may account for why the TCS SRO criterion overestimates the SRO in the DZ system. Further evidence that TCS SRO does not determine the packing efficiency in this system is provided by the relatively low density of the DZ system ($0.838\sigma^{-3}$) when compared to the WA ($1.291\sigma^{-3}$) or KA ($1.224\sigma^{-3}$) systems with the same cooling time ($t_{cool}=10\,000t_0$). Indeed, SRO that only considers icosahedral or-

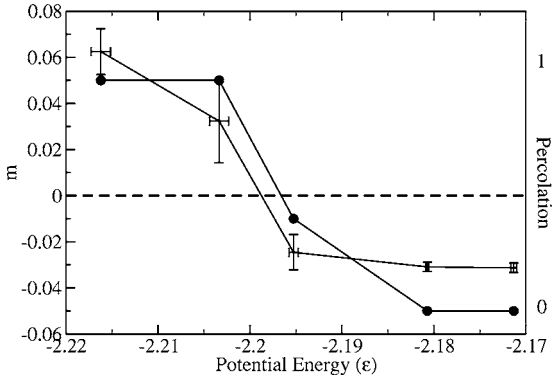

FIG. 8. The fraction of DZ systems that exhibit percolation (black dots) of icosahedral SRO is plotted as a function of potential energy per atom of each sample as measured prior to the mechanical test. The strain rate sensitivities for these systems, *m* (crosses), are also plotted for comparison.

der is observed to percolate near the mechanical behavior transition, as shown in Fig. 8. Similar percolation has been observed in the DZ system as the supercooled liquid approaches the glass transition.[64] For the WA system, we do observe a TCS SRO percolation transition to occur where the mechanical transition takes place as shown in Fig. 9. Therefore TCS SRO appears to be the relevant SRO for the WA system. For the KA system, no systems exhibited percolation. We believe this is not due to the lack of a structural transition, but rather due to the failure of TCS SRO to adequately characterize the KA system. Particularly, in this system the mean of the *AA* bond length and *BB* bond length is larger than that of the *AB* bond. Furthermore, the bond strength of *AB* is larger than that of either *AA* or *BB*, which indicates strong chemical affinity in this system. Therefore an alternative SRO that considers both the non-hard-sphere nature and the chemical SRO needs to be defined to reveal the structural transition that triggers the homogeneous-inhomogeneous deformation transition in this and similarly complex alloy systems where chemical effects play a significant role in determining bond lengths.

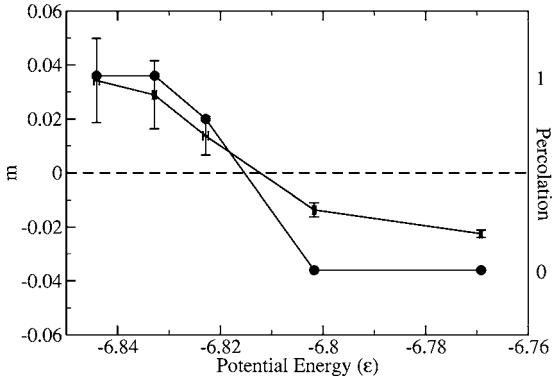

FIG. 9. The fraction of WA systems that exhibit percolation (black dots) of TCS SRO is plotted as a function of potential energy per atom of each sample as measured prior to the mechanical test. The strain rate sensitivities for these systems, *m* (crosses), are also plotted for comparison.

V. CONCLUSIONS

Using the Dzugutov system and two binary Lennard-Jones systems we have demonstrated that a number of our previous observations in two-dimensional systems also hold in these three-dimensional systems. In uniaxial compression tests of all three systems, strain localization is observed in glasses produced at lower cooling rates and homogenous deformation is observed in glasses produced at higher cooling rates. Moreover, the strain rate sensitivity of the localization changes from negative to positive which indicates an underlying transition from homogenous to localized deformation in the quasistatic limit as the quench rate is reduced.

We have generalized the Frank-Kasper criterion to determine the SRO in all three systems. This type of SRO originates from a model of efficient local packing of atoms given two important assumptions: that they interact only via near-neighbor interactions, and that efficiently packed structures consist of triangulated polyhedra. Therefore the appropriateness of this measure depends on whether the potential is similar in behavior to that of a hard-sphere system. Consequently the analysis achieved different levels of success in each of the glasses simulated. In the KA system the mean of the *AA* and *BB* bond lengths is significantly larger than the *AB* bond length, resulting in atoms deviating from spherical packing in heterogeneous chemical environments. The packing of nonspherical particles is significantly different than hard spheres because of the additional rotational degrees of freedom and can reasonably result in a deviation from triangulated coordination shells.[65] Therefore the KA system is the farthest away from the hard-sphere model. The maxima in the DZ potential introduces a significant second nearest-neighbor interaction that strongly favors the formation of icosahedra and other Frank-Kasper structures with coordination 14, 15, and 16 (Ref. 59) resulting in a high degree of distorted tetrahedral order. The fact that DZ system is less dense than a monatomic Lennard-Jones glass (approximately $1.0\sigma^{-3}$ using a similar quenching schedule), as well as the other two binary Lennard-Jones systems, indicates that this tetrahedral order is achieved at the expense of the packing efficiency. We believe this explains why DZ is observed to have a coinciding percolation point if only icosahedral order is considered, but exhibits excess SRO if the TCS SRO criterion is applied. The WA system is the closest to the hard-sphere model and we do observe a transition in percolation of TCS SRO corresponding to the mechanical transition in this system.

The key issue that emerges is the question of whether there is a unique way to define the most relevant measure of SRO in a general glassy system. A proper measure of SRO has to account for whether the structures in the material are energetically favorable but the generalized Frank-Kasper criterion we developed here only measures the packing geometry. For systems close to the hard-sphere model, this method should be a relevant measure of SRO in three-dimensional systems, even for larger size mismatch or more constituents. However, to the extent that actual bonding can vary significantly from the hard-sphere limit, this criterion is likely to break down in more complex alloy systems, and more sophisticated measures of short- and medium-range order will need to be developed.

ACKNOWLEDGMENTS

This work was supported by the National Science Foundation under Grant No. 0135009 and in part under Grant No. PHY99-07949. The authors would like to thank Michael Atzmon, Aaron Keys, John Kieffer, Naida Lacevic, Sharon Glotzer, and Daniel Miracle for stimulating discussions. We also thank the Center for Advanced Computing (CAC) at the University of Michigan for providing computational support.

[1] W. Sylwestrowicz and E. O. Hall, Proc. Phys. Soc. London, Sect. B **64**, 495 (1951).
[2] G. Debregeas, H. Tabuteau, and J. M. di Meglio, Phys. Rev. Lett. **87**, 178305 (2001).
[3] J. Lauridsen, M. Twardos, and M. Dennin, Phys. Rev. Lett. **89**, 098303 (2002).
[4] A. S. Argon, V. V. Bulatov, P. H. Mott, and U. W. Suter, J. Rheol. **39**, 377 (1995).
[5] F. Varnik, L. Bocquet, and J. L. Barrat, J. Chem. Phys. **120**, 2788 (2004).
[6] Y. L. Bai, J. Mech. Phys. Solids **30**, 195 (1982).
[7] M. A. Meyers, *Dynamic Behavior of Materials* (Wiley, New York, 1994).
[8] W. L. Johnson, MRS Bull. **24**, 42 (1999).
[9] M. F. Ashby and A. L. Greer, Scr. Mater. **54**, 321 (2006).
[10] C. A. Pampillo and H. S. Chen, Mater. Sci. Eng. **13**, 181 (1974).
[11] F. Spaepen, Acta Metall. **25**, 407 (1977).
[12] A. S. Argon, Acta Metall. **27**, 47 (1979).
[13] M. L. Falk and J. S. Langer, Phys. Rev. E **57**, 7192 (1998).
[14] P. S. Steif, F. Spaepen, and J. W. Hutchinson, Acta Metall. **30**, 447 (1982).
[15] H. Eyring, J. Chem. Phys. **4**, 283 (1936).
[16] M. L. Falk, J. S. Langer, and L. Pechenik, Phys. Rev. E **70**, 011507 (2004).
[17] C. A. Schuh, A. C. Lund, and T. G. Nieh, Acta Mater. **52**, 5879 (2004).
[18] H. S. Chen and S. Y. Chuang, Appl. Phys. Lett. **27**, 316 (1975).
[19] K. M. Flores, D. Suh, R. H. Dauskardt, P. Asoka-Kumar, P. A. Sterne, and R. H. Howell, J. Mater. Res. **17**, 1153 (2002).
[20] M. M. J. Treacy and J. M. Gibson, Acta Crystallogr., Sect. A: Found. Crystallogr. **A52**, 212 (1996).
[21] M. M. J. Treacy, J. M. Gibson, and P. J. Keblinski, J. Non-Cryst. Solids **231**, 99 (1998).
[22] J. M. Gibson and M. M. J. Treacy, Phys. Rev. Lett. **78**, 1074 (1997).
[23] P. M. Voyles, J. M. Gibson, and M. M. J. Treacy, J. Electron Microsc. **49**, 259 (2000).
[24] P. M. Voyles and D. A. Muller, Ultramicroscopy **93**, 147 (2002).
[25] J. Li, X. Gu, and T. C. Hufnagel, Microsc. Microanal. **9**, 509 (2003).
[26] W. H. Jiang and M. Atzmon, Acta Mater. **51**, 4095 (2003).
[27] J. Li, F. Spaepen, and T. C. Hufnagel, Philos. Mag. A **82**, 2623 (2002).
[28] J. Li, Z. L. Wang, and T. C. Hufnagel, Phys. Rev. B **65**, 144201 (2002).
[29] W. K. Luo, H. W. Sheng, F. M. Alamgir, J. M. Bai, J. H. He, and E. Ma, Phys. Rev. Lett. **92**, 145502 (2004).
[30] R. L. McGreevy, J. Phys. IV **111**, 347 (2003).
[31] H. W. Sheng, W. K. Luo, F. M. Alamgir, J. M. Bai, and E. Ma, Nature (London) **439**, 419 (2006).
[32] D. Deng, A. S. Argon, and S. Yip, Philos. Trans. R. Soc. London, Ser. A **329**, 549 (1989).
[33] D. Deng, A. S. Argon, and S. Yip, Philos. Trans. R. Soc. London, Ser. A **329**, 575 (1989).
[34] D. Deng, A. S. Argon, and S. Yip, Philos. Trans. R. Soc. London, Ser. A **329**, 595 (1989).
[35] D. Deng, A. S. Argon, and S. Yip, Philos. Trans. R. Soc. London, Ser. A **329**, 613 (1989).
[36] D. Srolovitz, T. Egami, and V. Vitek, Phys. Rev. B **24**, 6936 (1981).
[37] D. Srolovitz, V. Vitek, and T. Egami, Acta Metall. **31**, 335 (1983).
[38] K. K. Cameron and R. H. Dauskardt, Scr. Mater. **54**, 349 (2006).
[39] N. P. Bailey, J. Schiotz, and K. W. Jacobsen, Phys. Rev. B **73**, 064108 (2006).
[40] K. Brinkmann and H. Teichler, Phys. Rev. B **66**, 184205 (2002).
[41] F. Varnik, L. Bocquet, J. L. Barrat, and L. Berthier, Phys. Rev. Lett. **90**, 095702 (2003).
[42] M. J. Demkowicz and A. S. Argon, Phys. Rev. B **72**, 245205 (2005).
[43] Y. F. Shi and M. L. Falk, Phys. Rev. Lett. **95**, 095502 (2005).
[44] Y. F. Shi and M. L. Falk, Appl. Phys. Lett. **86**, 011914 (2005).
[45] D. R. Nelson and F. Spaepen, Solid State Phys., Adv. Res. Appl. **42**, 1 (1989).
[46] M. Dzugutov, Phys. Rev. A **46**, R2984 (1992).
[47] M. Dzugutov, Phys. Rev. Lett. **70**, 2924 (1993).
[48] F. H. M. Zetterling, M. Dzugutov, and S. I. Simdyankin, J. Non-Cryst. Solids **293**, 39 (2001).
[49] G. Wahnstrom, Phys. Rev. A **44**, 3752 (1991).
[50] N. Lacevic, F. W. Starr, T. B. Schroder, and S. C. Glotzer, J. Chem. Phys. **119**, 7372 (2003).
[51] F. Albano, N. Lacevic, M. L. Falk, and S. C. Glotzer, Mater. Sci. Eng., A **375-377**, 671 (2004).
[52] F. Albano and M. L. Falk, J. Chem. Phys. **122**, 154508 (2005).
[53] W. G. Hoover, Phys. Rev. A **31**, 1695 (1985).
[54] M. Parrinello and A. Rahman, J. Appl. Phys. **52**, 7182 (1981).
[55] M. Parrinello and A. Rahman, J. Chem. Phys. **76**, 2662 (1982).
[56] Y. F. Shi and M. L. Falk (unpublished).
[57] J. Roth and A. R. Denton, Phys. Rev. E **61**, 6845 (2000).
[58] M. H. McAdon and William A. Goddard, III, Phys. Rev. Lett. **55**, 2563 (1985).
[59] F. C. Frank and J. S. Kasper, Acta Crystallogr. **11**, 184 (1958).
[60] D. B. Miracle, W. S. Sanders, and O. N. Senkov, Philos. Mag. **83**, 2409 (2003).
[61] J. D. Honeycutt and H. C. Andersen, J. Phys. Chem. **91**, 4950 (1987).
[62] P. J. Steinhardt, D. R. Nelson, and M. Ronchetti, Phys. Rev. B **28**, 784 (1983).
[63] U. Gasser, A. Schofield, and D. A. Weitz, J. Phys.: Condens. Matter **15**, S375 (2003).
[64] M. Dzugutov, S. I. Simdyankin, and F. H. M. Zetterling, Phys. Rev. Lett. **89**, 195701 (2002).
[65] A. Donev, I. Cisse, D. Sachs, E. Variano, F. H. Stillinger, R. Connelly, S. Torquato, and P. M. Chaikin, Science **303**, 990 (2004).